Terrain analysis, erosion simulations and sediment fingerprinting: a case study assessing the erosion sensitivity of agricultural catchments in the border of the volcanic plateau of Southern Brazil

Alice Dambroz, Jean Minella, Tales Tiecher, Jean Moura-Bueno, Olivier Evrard, Fabricio Pedron, Ricardo Dalmolin, Felipe Bernardi, Fabio Schneider, Olivier Cerdan

Terrain analysis, erosion simulations and sediment fingerprinting: a case study assessing the erosion sensitivity of agricultural catchments in the border of the volcanic plateau of Southern Brazil

Alice P. B. Dambroz[1], Jean P. G. Minella[1], Tales Tiecher[2], Jean M. Moura-Bueno[1], Olivier Evrard[3], Fabricio A. Pedron[1], Ricardo S. D. Dalmolin[1], Felipe Bernardi[1], Fabio J. A. Schneider[1], Olivier Cerdan[4]

[1] Federal University of Santa Maria, Soil Department, Santa Maria, RS, Brazil
[2] Federal University of Rio Grande do Sul, Soil Department, Porto Alegre, RS, Brazil
[3] Laboratoire des Sciences du Climat et de l'Environnement (LSCE – IPSL), Unité Mixte de Recherche 8212 (CEA/CNRS/UVSQ), Université Paris-Saclay, Gif-sur-Yvette, France
[4] Bureau de Recherches Géologique et Minières (BRGM), Orléans, France
Corresponding Author: Alice P. B. Dambroz, e-mail: alice_pbd@outlook.com
ORCID: Alice P. B. Dambroz (https://orcid.org/0000-0003-0921-1034), Jean P. G. Minella (0000-0001-9918-2622), Tales Tiecher (0000-0001-5612-2849), Jean. M. Moura-Bueno (0000-0002-7240-3728), Olivier Evrard (0000-0002-3503-6543), Fabricio A. Pedron (0000-0002-5756-0688), Ricardo S. D. Dalmolin (0000-0002-8834-9869), Felipe Bernardi (0000-0002-7964-6474), Fabio J. A. Schneider (0000-0001-8406-6661), Olivier Cerdan (0000-0003-1395-3102)

Abstract

Purpose

Erosion and its spatial distribution in three agricultural headwater catchments were assessed in the border of the volcanic plateau in Southern Brazil. We analyzed terrain, hydrological processes and land use influence to provide a comprehensive assessment of the catchments' sensitivity to erosion.

Methods

Topographic attributes were acquired from a digital elevation map, WaterSed model was parametrized to simulate runoff, diffuse erosion and sediment yield, and sediment source contributions were estimated using sediment fingerprinting based on near-infrared spectroscopy.

Results

According to the modeled results, areas covered by crop fields, grasslands and those adjacent to the drainage network are the most sensitive to erosion. Short distances from the source to the river network and the occurrence of high magnitude rainfall events (80 mm) promoted increases in connectivity for runoff/sediment transfer. Erosion simulations show that areas of low infiltration, as unpaved roads, were important runoff generators during lower volume rainfall events (25 mm). Sediment fingerprinting provided satisfactory results to quantify the contributions of unpaved roads to sediment (~39%). Topsoil and stream channels were also significant sediment sources for the set of analyzed samples, corresponding to average contributions of 38 and 23%, respectively.

Conclusion

Areas sharing geomorphological similarities did not lead to similar sediment contributions. Vegetation cover controlled erosion in topographically sensitive areas. Unpaved roads provide a significant sediment source, followed by topsoil and stream channels. The complementary results provide useful insights to better coordinate planning environmental conservation strategies in these fragile landscapes.

Key-words Erosion sensitivity; Topographic attributes; GIS; WaterSed; Sediment fingerprinting; source to sink.

1 Introduction

Soil erosion is responsible for economic, social, and environmental damages occurring both on- and off-site (Boardman et al. 2019). There is an interest in understanding erosion processes to propose better management practices. These studies require long term monitoring data (Silva et al. 2021), which can be costly to acquire. Yet, there are tools to rapidly analyze an environment's fragility. Topographic attributes' analysis is a quick and useful tool for spatial representation of erosion susceptibility and zones prone to material loss and deposition (Moore et al. 1991; Wilson and Gallant 2000; Gruber and Peckham 2009; Vijith and Dodge-Wan 2019) for large areas with complex terrain. Advances in remote sensing (Karydas et al. 2014) and its data availability made it common to use models to estimate or predict soil erosion, providing a first look on the dynamic processes of soil degradation, runoff and erosion in an area of interest (Mitasova et al. 1996; Alewell et al. 2019; Teng et al. 2019). These approaches can be combined

with rapid monitoring techniques, such as fingerprinting (Martínez-Carreras et al. 2010), to quickly reflect the panorama of the spatial distribution of soil degradation.

The analysis of topographic attributes aims to address the natural variabilities of a landscape and can be used to propose the most appropriate practices for soil and water conservation, by reducing environmental impacts of agriculture. Its applicability to catchment scales has a main role to identifying risk areas and maintaining natural resources and environmental sustainability (Berry et al. 2005). Slope and the Stream Power Index are topographic attributes widely used in hydrology to characterize the spatial patterns of soil erosion (Mitasova et al. 1996; Ahmad 2018). This terrain analysis has been used for determining erosion susceptibility (Vijith and Dodge-Wan 2019) and identifying erosion hotspots (Mhiret et al. 2018). Although they may characterize both simple and complex terrain features, they do not reflect land use, climate and soil management practices' effects on catchment hydrology.

Since the erosive process is dynamic in time and space and dependent of other controlling factors, a more detailed analysis of an environment's fragility to erosion should be considered. Besides topography, rainfall characteristics, soil type, land use and management are also controlling factors of soil erosion, suggesting that – at the catchment scale – there is a need for a more complex analysis. For this reason, mathematical models combine a series of parameters (Merritt et al. 2003) to describe and to predict the occurrence of surface runoff and erosion according to changes in soil properties, rainfall patterns, and land use and management (Nearing et al. 2005). Empirical models (e.g., RUSLE) have been used for assessing erosion risk (Bezak et al. 2021) as they require relatively fewer input parameters, making the numeric solution objective, yet with a limited process description. Accordingly, physically-based distributed models provide an alternative tool for evaluating the spatial variability of erosion within a catchment, through the identification of erosion hotspots (Lemma et al. 2019).

Although the erosion processes occurring within a catchment reflect on sediment yield, material transfer from hillslopes to river systems also depends on landscape connectivity and depositional processes (Wohl et al. 2019). The complexity of processes and parameters that affect hillslope and bank erosion makes it difficult to quantify sediment supply from a catchment to a river channel (Julien 1995). To address this, the sediment fingerprinting technique (Haddadchi et al. 2013; Walling 2013; Collins et al. 2020) couples traditional sediment monitoring programs with tracing techniques to estimate sediment sources across the landscape (Evrard et al. 2011; Owens et al. 2016).

This approach provides a quantification of source contributions to sediment through the analysis of conservative bio-physico-chemical properties in potential source and target material. For this purpose, cost- and time-intensive conventional tracing properties (e.g., radionuclides, elemental and isotopic geochemistry), or simple and alternative methods as those relying on near-infrared spectroscopy coupled to statistical modelling were shown to be efficient in estimating land use source contributions to sediment yield (Verheyen et al. 2014; Tiecher et al. 2021).

Still, all the hydrological and erosion processes occurring within a catchment are not assured to be incorporated in a holistic approach or model that comprehends the series of phenomena occurring on variable and continuous ranges of scales (Gentine et al. 2012). For instance, to improve the understanding of erosion processes occurring from the source to the outlet of a catchment, sediment fingerprinting has been coupled to erosion modeling in target catchments (Palazón et al. 2016; Battista et al. 2020; Uber et al. 2021). Integrating techniques to provide multiple lines of evidence may increase the robustness of the erosion processes' assessment.

Therefore, a more accurate process representation should address the variabilities by coupling the analysis of these dynamic systems (Gentine et al. 2012). While hillslope processes may be addressed by terrain analysis and erosion modelling, sediment fingerprinting could enlighten the connection between them and the drainage network. To this end, the purpose of this study is to use complementary tools to evaluate the sensitivity to erosion and its spatial distribution in three environmentally fragile headwater catchments, nested within a heterogeneous catchment located along the border of the volcanic plateau in Southern Brazil, characterized by an intensive agricultural use and without continuous hydro sedimentological monitoring. Three approaches were analyzed including i) terrain analysis, ii) erosion modeling as a dynamic erosion index and iii) sediment fingerprinting to provide a comprehensive assessment of the sensitivity of these landscapes to erosion.

2 Materials and methods

2.1 Study area characterization

Guarda Mor catchment (Fig. 1), in Southern Brazil, is characterized by different land uses, soil types and lithology, and a complex terrain morphology. The average annual

rainfall is 1,940 mm, according to data collected from 2011 to 2020 at station number 2953008 (ANA 2021). The mean annual temperature is 19°C and climate is subtropical, type Cfa 2, according to Köppen's classification (Alvares et al. 2013).

Fig. 1 Location of Guarda Mor catchment, Júlio de Castilhos' rainfall-runoff monitoring station and ANA's weather station number 2953008 within the state of Rio Grande do Sul. In detail, soil and sediment sampling sites at Guarda Mor catchment.

Guarda Mor's main river monitoring station (GMex) drains a surface area of approximately 18.5 km², with elevation ranging from 194 to 511 meters (Fig. 2). A nearly levelled to very undulating relief is observed in its upper and lower segments, while its middle third is characterized by a basaltic escarpment. This catchment comprises three nested sub catchments with respective drainage areas of 2.1, 4.2 and 1.4 km², referred to as S1, S2 and S3 hereafter.

Located in a transition zone between the Meridional Plateau and the Central Depression of Rio Grande do Sul, GMex is characterised by a diverse geology (Wildner et al. 2008), as observed in Fig. 2. The Southern Plateau, in its upper segment, is underlain by volcanic rocks from the Serra Geral Group (Rossetti et al. 2018), including rocks from the Caxias sub-group (rhyodacite) and the Torres and Vale do Sol Formations (basalt). In the Central Depression (sedimentary basin), sandstones from the Botucatu and Caturrita Formations are found (Fig. 2).

Fig. 2 Guarda Mor catchment. **a** Digital elevation map. **b** Pedological and **c** geological maps. **d** Land use classification map.

This geological diversity led to the formation of several soil types (Fig. 2), which were mapped by Pedron et al. (2021). They include, according to the WRB classification System (IUSS Working Group WRB 2015), Leptosols, Nitisols, Cambisols, Gleysols, Regosols and Acrisols.

To create an annual land use map, the Difference Vegetation Index, Enhanced Vegetation Index, Normalized Difference Vegetation, Normalized Ratio Vegetation Index and soil adjusted vegetation index were derived from LANDSAT-8 satellite images. Field observation and Random Forest modeling (Breiman 2001) were used for building the map. The selected images were taken in April, September and December in 2019, so that seasonal changes in vegetation cover were well captured. Later, the main road segments were digitized manually using both satellite images and field observations.

According to the land use classification map (Fig. 2), forests occupy 44% of this catchment's area, followed by crop fields (39%), grasslands (11%), urban or pavement

areas (2%), unpaved roads (1%) and water bodies (1%). Forests are mostly located in the steepest portion of this catchment. In the upper segment of the headwater catchments, land use mainly consists of crop fields, where a succession of soybeans monoculture in summer and wheat or oats during winter are cultivated in a no-till system. Grasslands are areas under permanent pasture, without soil tillage nor sowing of seasonal crops.

Crop fields cover 60 and 63% of the area of S2 and S3, respectively. Forests occupy 21 and 20% of the area in each sub catchment, grasslands occupy 11 and 12% of the area and unpaved roads 2 and 1%. In S2 and S3, 1-2% of the area is covered by urban or paved areas, mainly farmhouses. In S1, crop fields are also the main land use (43%), forests occupy 33%, grasslands 16%, while paved/urban areas and unpaved roads occupy each 3% of its area. In S1 and S2 (Fig. 1), there are two crossing points between the drainage network and the roads, which have a total length close to 4500 and 5000 meters, respectively. In S3, the total road extension is less than 900 meters long and no crossing point is observed with the river drainage network.

2.2 Terrain analysis

Topographic attributes data were acquired for GMex, S1, S2 and S3 to spatially identify the main hotspots where erosion processes are strongly relief-influenced. Using a zonal statistics tool on QGIS v. 3.8.3 (QGIS Development Team 2020), data from the topographic attributes under each land use were extracted for every sub catchment, for its comparison and analysis.

An ALOS PALSAR Digital Elevation Model (DEM) (ASF DAAC 2010) was obtained with a spatial resolution of 12.5 m. It was downscaled to a resolution of 10 m for this study (Fig. 2), to avoid truncation errors during GIS' processes and overestimation of roads and stream channel's areas in the land use map. All maps were processed and obtained using the System for Automated Geoscientific Analyses (SAGA GIS v. 2.3.2) and QGIS v. 3.8.3 was used for organizing and preparing the final maps.

From the DEM, the following primary topographic attributes were obtained: a) slope, profile and plan curvatures calculated by the method of the 9th parameter 2nd order polynom (Zevenbergen and Thorne 1987); and b) catchment area using a recursive function. Zero value for profile or plan curvature indicates the occurrence of linear or planar surfaces, respectively. Negative profile curvatures represent convex surfaces and positive values, concave areas. Plan curvatures represent surfaces of convergent (negative

values) or divergent (positive values) flow. Slope and catchment area were used as input data for calculating the secondary topographic attributes: a) Topographic Wetness Index (TWI), following Beven and Kirkby's (1979) TOPMODEL; b) LS Factor, based on Moore et al. (1991) method; c) and Stream Power Index (SPI), also based on Moore et al. (1991). Frequency histograms using these data were organized for each sub catchment.

2.3 Soil erosion modeling

The goal of this approach was to parameterize an erosion model, that considers soil surface and land use characteristics, to provide a dynamic indicative of the catchments' erosion sensitivity in response to a storm rainfall event. Therefore, we chose the raster-based, spatially distributed and event-based WaterSed model (Patault et al. 2020; Grangeon et al. 2021). It was developed to model the spatial distribution of runoff and erosion from field to catchment scale. WaterSed is an upgrade of the STREAM model, which was designed to avoid over-parameterization and uncertainties in modelling (Cerdan et al. 2002). Spatially-distributed modelling approaches are adequate for understanding sediment transport, since every sediment source is characterized by different travel times (Merritt et al. 2003). Considering potential difficulties in representing processes or interpreting physical phenomena with equations and parameters without overloading model parametrization, WaterSed model represents an interesting compromise that permits to take into account the main erosion processes (infiltration, saturation, detachment by raindrop, detachment by runoff, deposition) with an adapted parameterization that is easily obtained (see Chabert (2019) for full explanation or Grangeon et al. (submitted)).

WaterSed's consistent conceptual structure includes a hydrologic and a sediment module, details on its equations are in Landemaine (2016). WaterSed presents a simple and efficient strategy for incorporating land use and management's effects on erosion and hydrological processes. Furthermore, it allows the incorporation of runoff's re-infiltration process, an important feature considering the study catchment. Runoff and sediment that reach the permanent river network are directly delivered to the lowest point downstream. The model results were used to analyze diffuse erosion processes occurring under each land use through the calculation of zonal statistics. The model does not allow the simulations of channel bank erosion and sediment storage within the channel; besides, in these sub catchments, channels run over bedrock with boulders and have stable margins.

The model is run using SAGA GIS and the input data is composed of decision tables and raster maps. The maps correspond to: DEM; stream network and channel width; soil type and land use. Each land use is then associated to soil surface characteristics based on decision tables, which allowed the parametrization approach used in this study. The tables (Cerdan et al. 2002a, 2002b) are built based on expert knowledge and adjusted to local conditions, according to each land use, to associate soil properties observed in the field to infiltration rates. They include Manning's roughness coefficient, a potential value for suspended sediment concentration (SSC), soil erodibility, infiltration rate and antecedent moisture content.

Although we do not have data from hydro-sedimentary monitoring in the study catchment to calibrate and validate WaterSed, we chose to parameterize it for modeling runoff volume, sediment yield and diffuse erosion in the three sub catchments. The data that was used in this parametrization was obtained from a runoff and SSC dataset we had access to. The data was monitored on hillslopes and zero-order catchments, where WaterSed was calibrated based on a robust database of water and sediment discharges. The site is a nearby field-scale, rainfall-runoff monitoring station in Júlio de Castilhos (Fig. 1). Detailed information on the site's characteristics and direct measurements' obtention can be found in Londero et al. (2021a, 2021b) and Schneider (2021). Further information is presented in Tables 1 and 2 in the supplementary material.

These parameters were used since both study areas are exposed to similar environmental conditions, considered to be representative of those occurring in Guarda Mor's headwater sub catchments. Values for Manning's roughness coefficient were defined based on Engman (1986). Default scale effect correction and recession time, flow width, critical runoff peak for rill erosion and sediment settling parameter coefficients were applied.

The model also requires information on rainfall depth and duration. The rainfall events we chose to simulate are based on events that generated significant runoff and were monitored in the nearby Júlio de Castilhos station (29°13'39"S, 53°40'38"W) (Londero et al. 2017; Londero et al. 2021a), their characteristics are described in Table 1.

2.4 Fine sediment fingerprinting

The origin of riverbed sediment was determined by a fingerprinting method based on NIR spectroscopy (Verheyen et al. 2014; Tiecher et al. 2016; Tiecher et al. 2021) and

modeling with Support Vector Machine (SVM) to build spectroscopic models of sediment estimation (Tiecher et al. 2021). Two source groupings (by land use and by sub catchment) were considered as potential end-members to analyze the spatial variability and the main erosion processes to explain the sediment yield observed at the outlets.

The first approach was based on spatial sources and the three headwater sub catchments were considered as end-members. The objective of this so-called tributary approach was to indicate which sub catchment contributed with greater amounts of sediment that reached the GMex's outlet. The second approach considered land use source types (including topsoil, forest, unpaved roads, and stream channel) within each sub catchment, with the objective to outline which land uses or landscape components were contributing with more sediment to S1, S2 and S3's outlets. Therefore, sediment samples were both, alternatively, used as sources and target material, whether they were considered in the first or second approach, respectively.

2.4.1 Soil and sediment sampling and analysis

Potential sediment sources were sampled based on visual field evidence of erosion or soil degradation and connectivity to the drainage network, in each sub catchment. The soil samples were collected from crop fields, grasslands, stream channels, forests, and unpaved roads. Due to sample similarities that led to low discrimination of sources, samples from crop fields and grasslands were grouped as topsoil source, such as Poulenard et al. (2009) and Verheyen et al. (2014) also did. Each sample was composed by five sub-samples that were mixed and homogenized to compose a representative sample (Table 2). They were collected on the soil surface (0–2 cm depth), due to the higher likelihood of surface material to be mobilized by water erosion.

Sediment deposited on the riverbed were sampled along the river channels at the outlets of S1, S2, S3 and at GMex, between January and June in 2019. Care was taken during the sediment sample collection process to avoid losing fine material.

All samples were oven-dried with forced air circulation and at a temperature between 40 and 50°C. Then, samples were gently disaggregated and sieved at 63 µm, to minimize particle size differences between samples (Laceby et al. 2017), and between potential sources and sediment material. Afterwards, all samples were analyzed by near-infrared spectroscopy. The spectra range from 12,000 to 4,000 cm^{-1} was scanned, using the Bruker MPA FT-NIR (Fourier transform near-infrared) spectrometer, at a resolution

of 2 cm^{-1}. Samples were carefully placed in a Petri dish prior to scanning and background readings were regularly performed.

2.4.2 Building spectroscopic models to estimate sediment source contributions

To calibrate the prediction models and test the analyzed properties' additive behavior, artificial mixtures (Poulenard et al. 2009) were prepared in the lab using source samples. The set of mixtures was designed to account for spectral diversity, and it was used for calculating the model's confidence statistics by testing its performance. First, samples of each potential source were mixed in equal weight proportions to compose one reference sample. Then, from these, other mixtures were created by mixing them in different proportions to build the statistical model. For the tributary approach, 37 artificial mixtures were created with the sediment samples collected from each sub catchment. Their distribution can be visualized in a ternary diagram (Fig. 1 in the supplementary material). For the land use approach, 72 artificial mixtures were created covering a range from 0 to 100% of each potential source sample (Table 3 in the supplementary material).

The spectra dataset was transformed by a smoothing and data derivative algorithm, Savitzky-Golay derivative, first-order polynomial (11 window points) (Savitzky and Golay 1964). By calculating the first derivative, this pre-processing calculates the change rate between absorbance and wavelength, highlighting the occurrence of bands. This was performed using the R package "prospectr" (Stevens and Ramirez-Lopez 2013).

Then, for establishing a relationship between spectral data (x variable) and the contribution of a given source (y variable), SVM models (package e1071 – Meyer et al. 2019) were adjusted. The SVM is a non-parametric model and was run with the kernel function, which separates the calibration data into hyperplanes and seeks to establish correlations between the dependent and independent variables when these have non-linear behavior (Ivanciuc 2007). The kernel function seeks to establish correlations between the reflectance value and the target variable, in which the model seeks to identify a interpolation function between the variables and creates support vectors, a robust procedure in statistical learning models (Ivanciuc 2007). This type of model was selected due to the occurrence of non-linear correlations between the organo-mineral components of soils/sediments and the spectral variables (Viscarra Rossel and Behrens 2010) and given the acquisition of more accurate estimates using this model in comparison, for

example, to parametric models Partial Least Square Regression (PLSR), by Tiecher et al. (2021).

Data from the artificial samples was randomly separated among calibration and validation sets. Each model was calibrated with 70% of the samples (n = 26 and 51, tributary and land use approaches) and validated with the remaining 30% of the samples (n = 11 and 21, tributary and land use approaches). A total of 15 SVM regression models were independently calibrated, one for each sediment source. No boundary conditions to avoid results lower than 0 or higher than 100% were set for the models. The models were used for predicting the contribution of each potential source to the individual sediment samples.

To evaluate model accuracy, the following parameters were calculated: coefficient of determination (R^2), mean error (ME) and mean square root of the prediction error (RMSE). The spectral wavelengths of the sediment samples collected at the four outlets were submitted to a principal component analysis (PCA) and hierarchical clustering on principal components (package Factoshiny – Vaissie et al. 2020) for visualizing the differences in samples used in the tributary approach.

3 Results and discussion

3.1 Terrain analysis

The spatial distribution of the TWI, SPI and LS Factor is found on Fig. 3. Results of the terrain analysis are presented by subdividing potential erosion zones in different sensitivity value classes and according to the different land uses.

Fig. 3 Maps of Topographic Wetness Index (TWI), Stream Power Index (SPI) and LS Factor.

In S1, 40% of the area has slopes between 8 and 20% (Fig. 4). S2 is the gentlest sub catchment, around 60% of its area has low-levelled slopes (0 to 8%). Flat slopes occupy less than 10% of S3's area and 40% of the hillslopes range from 8 to 20%. Steeper slopes are located closer to the streams in both S1 and S3. Forests are found in steep areas of S1 and S3, as well as grasslands and crop fields, although in different proportions.

Fig. 4 Frequency histograms for Topographic Wetness Index (TWI), LS Factor, Stream Power Index (SPI) and Slope of sub catchments and GMex.

Flat profile curvatures occupy 45, 47 and 44% of the area of S1, S2 and S3, respectively. Convex and concave surfaces correspond each to around 27% of their areas. Regarding plan curvatures, 96% of the area of S1 and S2, and 94% of S3's, are occupied by planar surfaces. Divergent curvatures correspond to 1% of the sub catchments' areas. Convergent curvatures correspond to 3% of S1 and S2's surfaces and 4% in S3. In all sub catchments, crop fields are the land use with the most convergent surfaces (Fig. 5), except for unpaved roads in S2. The most divergent surfaces are forests in S1 and S3, followed by grasslands. In S3, the most divergent surfaces are over crop fields and grasslands.

Fig. 5 Boxplots of zonal statistics analysis for topographic attributes (LS Factor, Slope, Stream Power Index – SPI, Topographic Wetness Index – TWI and Plan Curvature) and land uses in sub catchments 1, 2 and 3.

TWI ranged from around 5.5 to 21 in the sub catchments (Fig. 4). S1 and S3 have similar TWI range distribution, and S2 has a larger area of higher TWI. Stream channels have the highest median TWI values. Overall, TWI distribution among land uses is similar (Fig. 5).

SPI ranged from 0 to around 290,000 in S1, to 340,000 in S2 and to 170,000 in S3. Nearly 99% of the sub catchments' areas have values corresponding to less than 10,000. Therefore, greater differences are observed in the remaining area, for which data were separated into five classes (Fig. 4) in each sub catchment and GMex. S1 shows a tendency to increased soil erosion per area, given its greater percentage of higher SPI values. In S1, the highest SPI values are found in crop fields followed by forests, grasslands and stream channels (Fig. 5). As S2 has a greater drainage area, it reaches higher SPI values. Grasslands reach the highest SPI values in S2, followed by forests and crop fields. Unpaved roads also reach the highest value in S2. While in S3, the crop fields and stream channels reach the highest values, followed by forests.

LS factor ranged from 0 to 27 in S1, 0 to 18 in S2 and 0 to 19 in S3 (Fig. 5). Higher values were found closer to the drainage network. S1 and S3 show dense areas with higher values due to the combination of high steepness and slope length in these zones, explaining their high potential for erosion and material transport. Stream channels, grasslands and forests in S1 are land uses that showed some of the highest LS Factor values (Fig. 5). In S2, forests reach the highest value for this attribute. Given the LS factor range, crop fields in S3 are likely more sensitive to erosion than in S1 and S2.

Most of the areas with steeper slopes in these sub catchments are occupied by forests. Dense vegetation covers, such as those observed in forests, can intercept part of

the precipitation (Sari et al. 2016). This can delay the time for soil infiltration to be exceeded and limit runoff rates. Slope analysis results show that S2 tends to have a lower punctual erosive capacity than S1 and S3. S1 and S3 share some similarities in the ranges of these indexes. Besides having a general tendency to increases in flow speed, given its steeper slopes (Wilson and Gallant 2000), the presence of shallow soils (Fig. 2) may also lead to greater surface runoff (Brosens et al. 2020).

A few larger zones of planar and linear curvature, which coincide with segments of lower SPI values and high TWI values (Fig. 3), underline the occurrence of zones where runoff and sediment may accumulate. Although higher TWI values may be representative of overland flow connectivity in a catchment, isolated areas of higher TWI are also indicative of hydrological sinks and disconnectivity or discontinuity in sediment and runoff transfer, favoring sediment deposition (Jancewicz et al. 2019). S2 has larger area of higher TWI values than the other two sub catchments (Fig. 4). Yet, SPI differences among the sub catchments indicate that S2 has a higher runoff energy.

On hillslopes, higher TWI values can also indicate that these areas are more prone to concentrated forms of erosion. For instance, Momm et al. (2012) used TWI to identify the location of ephemeral gullies, Mihret et al. (2018) also found TWI to be successful in predicting gully formation, along with SPI. In addition, Vijith et al. (2019) determined that slope, SPI and the LS factor were some of the most crucial variables to predict erosion susceptibility in a catchment. Mapping these variables provides a prerequisite to implementing precision conservation, for soil and water conservation (Berry et al. 2005). In Fig. 6 TWI and SPI maps over satellite images of crop fields of GMex show concentrated forms of erosion corresponding to higher values of these indexes.

Fig. 6 Comparison between higher TWI (a and b) and SPI (c and d) values and satellite images in crop fields of sub catchment 1.

By this analysis, the most fragile zones are associated with crop fields, grasslands and near the drainage network (Fig. 3). High index values were observed at upper catchment locations on unpaved roads, a landscape component known to be prone to runoff generation (Ziegler et al. 2000), such as crop fields are (Londero et al. 2017).

3.2 Erosion modeling

For each event (Table 1), only precipitation volume, rainfall duration and imbibition were altered. Increases in volume and magnitude enhanced modeling outputs'

441 visualization in terms of runoff and sediment production's spatial distribution (Fig. 7).
442 Since we did not calibrate nor validate the model and used this analysis as a runoff/erosion
443 sensitivity index, results should be carefully interpreted as erosion estimates.

444 **Fig. 7** WaterSed output maps for runoff and erosion in the three sub catchments,
445 for events 1, 2, 3 and 4.

446 The values for surface runoff (m^3) and sediment yield (kg) simulated at the outlet
447 of each sub catchment, and the maximum values for diffuse erosion (kg) observed within
448 each sub catchment are found in Table 4 in the supplementary material. Simulated runoff
449 and sediment yield of S2 were systematically the highest. S1 and S3 had, respectively,
450 the overall second highest and lowest amounts of runoff and sediment yield at their
451 outlets. The maximum erosion was observed in S2, followed by S1 and S3.

452 The spatial distribution of runoff increases the connectivity from upper segments
453 occurring in these catchments. The simulation of event 4 (Fig. 7), a lower volume rainfall,
454 shows lower runoff volumes. Flow on hillslopes was less connected to streams, but
455 unpaved roads provided significant zones of runoff generation. On the contrary, greatest
456 volume and magnitude from event 2 reflected on an enhanced connectivity.

457 Greater rainfall volumes led to increased sediment yield. The highest amounts
458 were obtained for S2. Despite the event's magnitude, the highest sediment yield for S1
459 and S3 were not observed at their outlets, but at upper catchment locations. S1 reached
460 higher values than S3, except for event 2. Higher values observed far from S1 and S3's
461 outlets can be attributed to runoff re-infiltration or sediment deposition calculated by the
462 model (Landemaine 2016). Considering the simulated values at the outlets, results
463 indicate S2's greater fragility, due to higher sediment yield, runoff and sediment
464 connectivity.

465 As for diffuse erosion, greater rainfall volumes led to greater amounts of erosion.
466 The zonal statistics analysis (Fig. 8) showed that crop fields are the most erodible land
467 use in all sub catchments, especially in S2 and S3. In S1, both forests and grasslands were
468 also prone to erosion. Paved areas and unpaved roads showed higher erosion proportions
469 in S1 than in S2 and S3. The opposite result was observed for stream channels.

470 **Fig. 8** Zonal statistics for diffuse erosion estimates and land uses in sub
471 catchments 1, 2 and 3.

472 With greater catchment area, S2 showed the greatest potential for runoff, sediment
473 yield and diffuse erosion. The maps (Fig. 7) indicate that unpaved roads can rapidly
474 generate runoff, even during low-intensity events. For greater rainfall volumes, the most

sensitive areas are located near the headwaters, in the vicinity of the drainage network and steepest areas, similarly to the observations from terrain analysis.

3.3 Sediment fingerprinting

Calibration results and the associated statistical metrics showed a good performance of the different models, although validation results showed large variations in model performance. These results are shown in Table 3. Models for unpaved roads and forests were the best in every sub catchment, with R^2 between 0.99 and 1.00 for calibration, and between 0.71 and 0.93 for validation, indicating their good discrimination of these sources. For all models, summed predictions reached totals slightly greater than 100%, in line with the overestimation observed by Poulenard et al. (2009) and attributed to differences in soil and sediment material used for model calibration and prediction.

Since NIR range of soil spectra is influenced by different soil organic and mineral constituents (Viscarra Rossel et al. 2006), forest models could have presented better results due to highest organic matter content among the potential sources, resulting in better distinction and model performance (Brosinsky et al. 2014). Low organic matter content on unpaved roads may be responsible for their good discrimination, as observed by Tiecher et al. (2016, 2021).

In contrast, model validation for topsoils showed R^2 results ranging from 0.28 to 0.36. This may be due to great variability in the sample material or insufficient sampling to represent this source. Regarding stream channel contributions, Tiecher et al. (2016) associated this source's good discrimination to the fact that soils located near the drainage network are subject to biogeochemical alterations due to oxi-reduction reactions, leading to a different mineral composition and, therefore, different spectral features.

Regarding sediment source contributions in S1, topsoil, unpaved roads and forest showed variable sediment supply throughout time (Fig. 9). Stream channels displayed the lowest variations in their contributions. A single sample presented 50% of the sediment contribution originating from unpaved roads. This source supplies a mean contribution of 41%. Stream channels showed almost constant contributions to sediment, with an average 28% contribution. Finally, forests had the lowest sediment contribution (mean: 8%).

Fig. 9 Boxplots for sediment source contribution in Fingerprinting 1 (**a**) and Fingerprinting 2 (**b** = S1, **c** = S2, **d** = S3).

S2 had the lowest average forest contribution to sediment (mean: 1%). Unpaved roads were the highest sediment source in S2, with an average of 50% and a maximum contribution of 60% in an individual sample. Average agricultural topsoil contribution was 27%. Stream channel sediment contribution varied from 15 to 38%, averaging 23%.

Unlike the previous sub catchments, the main sediment source for S3 was topsoil (mean: 59%), followed by unpaved roads (mean: 24%). Stream channel had the lowest contribution to sediment (mean: 18%) compared to the other sub catchments, varying between 5 and 20%. Average forest contributions were lower than 7%.

There is a variation among the main sediment sources in the three sub catchments and a significantly high contribution from unpaved roads in all of them (Fig. 9), especially in S2. Stream channels also supplied a similar contribution (~ 23%) to sediment in all catchments, although in lower proportions (18%) in S3 where the topsoil contribution was higher (59%) than in S1 and S2.

Given S1's lower topsoil contribution, crop fields might not have contributed with much sediment due to soil management based on no-till. As demonstrated by Londero et al. (2017) and Deuschle et al. (2019), no-till's permanent biomass over the soil surface protects it against erosion, decreasing sediment yield from agricultural plots. Although vegetation cover may decrease sediment yield from crop fields, runoff may have concentrated along hillslopes, leading to greater contributions from downstream landscape components from the crop fields and grasslands, such as stream channels.

The lowest contribution from unpaved roads in S3 could be due to fewer road segments within its drainage area, compared to S1 and S2, and to their location in the upper portion of the sub catchment (Fig. 1).

Regarding tributary sediment contributions at GMex station (Fig. 9), on average, almost 90% of sediment originated from S1 with a low contribution from S3. Contribution from S2 ranged from 10 to 29%. Negative results found for S3 and its poor validation results outline the need for analysing more powerful tracers to achieve a better discrimination between sub catchments in the future. These contrasted results may also be attributed to the large differences in geology and soil types found downstream from the sub catchment's outlets and the characteristics of significant sources that could not be sampled in the current research. This variation in geology and soil contributes to increasing the variation in spectral data used to develop the estimation models. In addition, the spectral data of the present study represents only the near-infrared region, which is also a factor that results in less accurate estimates of sediment sources (Tiecher

et al. 2021). In the future, a denser sampling should be performed for better characterizing sources drained by tributaries. Associated with this, spectral data in the visible and mid-infrared regions should be used to improve the characterization of the organic and mineral constituents of the sediment sources.

According to the PCA, sediment samples from S1, S2 and S3 are located close to each other in the first dimension, in which the percentage of explained variance in the dataset reaches 87.27%. Samples from S2 separate well from S1 and S3 in the second dimension, explaining 9.94% of the variance. However, the samples from GMex were also well separated from those of the sub catchments in both dimensions (Fig. 10), which means that other sub catchments may be contributing to the sediment load at GMex.

Fig. 10 Individuals factor map from Principal Components Analysis for sediment samples for the outlets of sub catchments 1, 2 and 3, and GMex.

A hierarchical cluster analysis separated the samples from GMex in a first cluster, and from S1, S2 and S3 in a second one. This shows there is a significant difference between sediment samples collected at GMex and at the upstream catchments. Again, this highlights the need to monitor unsampled regions within GMex, where the contribution of additional sources may dilute that of the three sub catchments considered here.

3.4 The complementarity of tools to understand the erosive process

Terrain analysis and erosion modeling simulations' distribution of erosion-prone areas in the sub catchments demonstrates that they are mainly located in crop fields and near the streams, especially under grasslands and forests. Sediment fingerprinting results further increased the knowledge on these catchment's terrain and erosion modeling analysis, as it provided additional information on the significant contribution of unpaved roads on sediment contribution.

The most fragile areas to erosion are those located near the drainage network, similarly to what Capoane (2019) observed when assessing the erosion susceptibility of a Brazilian catchment. There appears to be some disconnectivity between landscape components and the drainage network among the sub catchments. Hotspots located near the drainage channels can accumulate upstream runoff and run-on and connect them to the river channel (Bracken and Croke 2007). Hydrological connectivity is most likely to exist where distances from hillslope to channel are shorter (Bracken and Croke 2007). Those spots can also be associated with the formation of rill and gully erosion, which act

as pathways for runoff to concentrate and be delivered with high transport and erosive energy to the drainage network.

Forests are found in areas with steep slopes and higher values for LS Factor and SPI, and they could be considered as very fragile. Erosion modeling outputs showed that forests in S1 were slightly more erodible. Yet, according to modelling, forests have a lower erosion potential and sediment fingerprinting showed that this land use provided very low sediment contributions in all sub catchments. This demonstrates the role of vegetation control on catchment degrading processes (Qiu et al. 2014).

Sediment fingerprinting results, such as those obtained by Tiecher et al. (2018) in an agricultural catchment of Southern Brazil, showed high sediment contributions from topsoil and stream channels. Topsoil contribution was the highest in suspended sediment samples (Tiecher et al. 2018), so future studies in this catchment should also collect and analyze samples in the water column taken in the rivers during flow events.

Sediment contribution from stream channels could be due to runoff leaving crop fields and grasslands with sufficient energy to erode riverbanks and to transport sediment from these sources. As this source was not simulated by WaterSed, it is difficult to directly compare results obtained with the different methods, which leads to uncertainty. Other uncertainties are related to the unsampled area between the sub catchments' and GMex's outlets, which would incorporate the different soils found within this catchment.

S1 is likely the sub catchment with the most sensitive zones to erosion, according to terrain analysis. According to erosion modeling, it had the second greatest simulated sediment yield and runoff, whereas tributary sediment fingerprinting results showed it supplied the highest sediment contribution to GMex. Regarding S3's sediment fingerprinting, the greater contributions originated from topsoil, as higher SPI and LS Factor values were observed in its crop fields. This is a major distinction compared to observations in S1 and S2, where the greatest sediment contribution was from unpaved roads. So, for S3, it can be concluded that terrain analysis provided a good representation of the erosion processes caused by overland flow across topographically fragile areas.

Based on these attributes, S1 and S3 showed a somewhat similar geomorphological organization, with the same dominant soil classes. Sediment samples collected at their outlets were also grouped together by the PCA, demonstrating a similar data variance. Yet, they behave differently when considering erosion modeling and sediment fingerprinting results, with S1 sharing more similarities with S2 than S3, demonstrating the impact of land use to control the sensitivity to erosion. Although S2

apparently had the highest disconnectivity caused by sinks, evidenced by terrain analysis, erosion modeling showed that this sub catchment had the greatest potential for runoff exported at the outlet. And the highest simulated sediment yield values were observed at its outlet, in contrast to the observation of maximum sediment yield at upper locations in S1 and S3, where significant sediment deposition occurred before reaching the outlet.

In S1 and S2, sediment contributions from topsoil and stream channels were found to be high, although a great proportion of sediment originated from unpaved roads. This confirms previous results obtained when calculating the sediment budget in a small catchment of Southern Brazil, where, despite occupying a minor proportion of the surface area, roads provided a significant sediment source contribution, supplying around 36% of the sediment to the river system (Minella et al. 2014). Also in Southern Brazil, Thomaz and Peretto (2016) found unpaved roads to have contributed with 70 to 87% of SSC in a headwater catchment. Unpaved roads have great potential for generating deleterious environmental impacts (Silva et al. 2021), such as increased runoff generation (Ziegler et al. 2000) and SSC in rivers, especially in small order streams (Thomaz et al. 2013).

From terrain analysis, we can interpret erosion sensitivity from a topographic point of view, but this is not the only erosion controlling factor in these catchments. Therefore, we benefit from combining approaches as we add information on more controlling factors to increase our understanding of complex natural phenomena. Modelling incorporates the climate, soil and land use influence over erosion, as well as its spatial distribution. In S1, for instance, there are steep slopes and high LS Factor and SPI values near the drainage network and the erosion modelling results corroborate with them, showing greater diffuse erosion in grasslands and forests, which occupy that area. Yet, although terrain analysis would not reflect a great erosion sensitivity from unpaved roads, modelling does show their importance as areas of limited infiltration that generate runoff even during low magnitude rainfall events, promoting constant runoff and sediment mobilization.

Still, there is great complexity regarding the connection between hillslope and river channel in terms of sedimentation (Walling 1983). The greatest diffuse erosion in S3 was from crop fields, as topsoil was the main sediment source of that catchment. Yet, while modeling outputs for stream channel and unpaved roads were not as significant, they are important sediment sources in S1 and S2, for instance. Sediment fingerprinting reflects the integration of all erosion processes occurring in a catchment and, although

modelling added insights to the understanding of soil erosion, it may not be sufficient to reflect the connectivity of a catchment (Wohl et al. 2019, Uber et al. 2021).

These complementary methodologies led to results with contrasted levels of information, including basic and advanced techniques. They address different individual erosion processes, from local to landscape observations and from the dynamic response of hydrological and erosion processes during individual rainfall events to their integration controlling the sediment yield at the catchment outlet. Despite the results model outputs, the consistence and the added value of their insights provides evidence that there is potential for validating the sediment fingerprinting results once erosion model outputs are validated based on continuous river flow and sediment monitoring data.

5 Conclusions

Combining terrain, erosion modelling and sediment fingerprinting analyses provided complementary insights into sediment dynamics in the region along the border of the Southern Brazilian basaltic plateau. Terrain analysis and erosion modelling outlined the specific fragility of crop fields, grasslands and areas located near the drainage network, characterized by high connectivity to the river system, increasing material/sediment transfer. When modeling greater rainfall intensity events, these areas appeared to expand. Geomorphological similarities in sub catchments did not lead to similar sediment contributions. This demonstrated the impact of vegetation cover to control erosion in topographically sensitive areas. Unpaved roads supply important sediment sources, followed by topsoil and stream channels, while forests showed negligible contribution. Combining different environmental diagnosis techniques was effective to outline the fragility of those areas where overland flow may accumulate and lead to accelerated processes of soil degradation. Despite its limitations, sediment fingerprinting provided very useful results that were confronted with those obtained from the more classical terrain analysis and erosion simulations through the quantification of sediment contributions from contrasted tributaries. The obtained information should be useful to the public managers to guide the implementation of effective soil erosion control measures across the landscapes of this environmentally fragile region of South America.

Acknowledgments The authors would like to thank the financial support from the National Council for Scientific and Technological Development – CNPq, Project No.

437523/2018-7. The authors are grateful to the Laboratório Federal de Defesa Agropecuária (LFDA Porto Alegre, RS) for allowing the NIR spectral readings.

Declarations

Funding This study was financially supported by the National Council for Scientific and Technological Development – CNPq (grant number 437525/2018-7).

Conflicts of interest/Competing interests The authors declare that they have no conflict of interest that are relevant to the content of this article.

Availability of data and material Data and material will be made available on reasonable request.

Code availability Code will be made available on reasonable request.

References

Agência Nacional de Águas (ANA) (2021) Hidroweb. https://www.snirh.gov.br/hidroweb/serieshistoricas

Ahmad I (2018) Digital elevation model (DEM) coupled with geographic information system (GIS): an approach towards erosion modeling of Gumara watershed, Ethiopia. Environ Monit Assess 190(10):568 https://doi.org/10.1007/s10661-018-6888-8

Alewell C, Borrelli P, Meusburger K, Panagos P (2019) Using the USLE: Chances, challenges and limitations of soil erosion modelling. Int Soil Water Conserv Res 7(3):203-225 https://doi.org/10.1016/j.iswcr.2019.05.004

Alvares CA, Stape JL, Sentelhas PC, de Moraes Gonçalves JL, Sparovek G (2013) Köppen's climate classification map for Brazil. Meteorol Z 22(6):711-728 https://doi.org/2010.1127/0941-2948/2013/0507

ASF DAAC (2010) Hi-Res Terrain Corrected; Includes Material © JAXA/METI 2010. Accessed through ASF DAAC 2019. https://doi.org/10.5067/Z97HFCNKR6VA

Battista G, Schlunegger F, Burlando P, Molnar P (2020) Modelling localized sources of sediment in mountain catchments for provenance studies. Earth Surf Process Landf 45(14):3475-3487 https://doi.org/10.1002/esp.4979

Berry JK, Delgado JA, Pierce FJ, Khosla R (2005) Applying spatial analysis for precision conservation across the landscape. J Soil Water Conserv 60(6):363-370

710 Beven KJ, Kirkby MJ (1979) A physically based, variable contributing area model of
711 basin hydrology/Un modèle à base physique de zone d'appel variable de l'hydrologie du
712 bassin versant. Hydrol Sci J 24(1):43-69 https://doi.org/10.1080/02626667909491834
713 Bezak N, Mikoš M, Borrelli P et al (2021) Soil erosion modelling: A bibliometric
714 analysis. Environ Res 197:111087 https://doi.org/10.1016/j.envres.2021.111087
715 Boardman J, Vandaele K, Evans R, Foster ID (2019) Off- site impacts of soil erosion
716 and runoff: Why connectivity is more important than erosion rates. Soil Use
717 Manag 35(2):245-256 https://doi.org/10.1111/sum.12496
718 Boudreault M, Koiter AJ, Lobb DA, Liu K, Benoy G, Owens PN, Danielescu S, Li S
719 (2018) Using colour, shape and radionuclide fingerprints to identify sources of sediment
720 in an agricultural watershed in Atlantic Canada. Can Water Resour J 43(3) :347-365
721 https://doi.org/10.1080/07011784.2018.1451781
722 Bracken LJ, Croke J (2007) The concept of hydrological connectivity and its
723 contribution to understanding runoff- dominated geomorphic systems. Hydrol Process:
724 Int J 21(13):1749-1763 https://doi.org/10.1002/hyp.6313
725 Breiman L (2001) Random Forests. Mach Learn 45:5-32
726 https://doi.org/10.1023/A:1010933404324
727 Brosinsky A, Foerster S, Segl K, Kaufmann H (2014) Spectral fingerprinting: sediment
728 source discrimination and contribution modelling of artificial mixtures based on VNIR-
729 SWIR spectral properties. J Soils Sediments 14(12):1949-1964
730 https://doi.org/10.1007/s11368-014-0925-1
731 Brosens L, Campforts B, Robinet J, Vanacker V, Opfergelt S, Ameijeiras- Mariño Y,
732 Minella J, Govers G (2020) Slope gradient controls soil thickness and chemical
733 weathering in subtropical Brazil: understanding rates and timescales of regional
734 soilscape evolution through a combination of field data and modeling. J Geophys Res
735 Earth Surf 125(6) https://doi.org/10.1029/2019JF005321
736 Capoane V (2019) Susceptibilidade a erosão na bacia hidrográfica do córrego
737 Guariroba, Campo Grande, Mato Grosso do Sul. Acta Bras 3(2):49-55
738 https://doi.org/10.22571/2526-4338180
739 Cerdan O, Le Bissonais Y, Couturier A, Saby N (2002a) Modelling interrill erosion in
740 small cultivated catchments. Hydrol Process 16(16):3215-3226
741 https://doi.org/10.1002/hyp.1098
742 Cerdan O, Souchère V, Lecomte V, Couturier A, Le Bissonnais Y (2002b)
743 Incorporating soil surface crusting processes in an expert-based runoff model: sealing

744 and transfer by runoff and erosion related to agricultural management. Catena 46(2-
745 3):189-205 https://doi.org/10.1016/S0341-8162(01)00166-7
746 Chabert C (2019) Modélisation distribuée de l'aléa érosif dans le bassin versant de la
747 Loire et nouvelles perspectives de validation. Thesis, Université Paris-Saclay
748 Collins AL, Blackwell M, Boeckx P et al (2020) Sediment source fingerprinting:
749 benchmarking recent outputs, remaining challenges and emerging themes. J Soils
750 Sediments 20(12):4160-4193 https://doi.org/10.1007/s11368-020-02755-4
751 Deuschle D, Minella JPG, Hörbe TAN, Londero AL, Schneider FJA (2019) Erosion and
752 hydrological response in no-tillage subjected to crop rotation intensification in southern
753 Brazil. Geoderma 340:157–163 https://doi.org/10.1016/j.geoderma.2019.01.010
754 Engman ET (1986) Roughness coefficients for routing surface runoff. J Irrig Drain
755 Eng 112(1):39-53 https://doi.org/10.1061/(ASCE)0733-9437(1986)112:1(39)
756 Evrard O, Navratil O, Ayrault S, Ahmadi M, Némery J, Legout C, Lefèvre I, Poirel A,
757 Bonté P, Estever M (2011) Combining suspended sediment monitoring and
758 fingerprinting to determine the spatial origin of fine sediment in a mountainous river
759 catchment. Earth Surf Process Landf 36(8):1072-1089 https://doi.org/10.1002/esp.2133
760 Gentine P, Troy TJ, Lintner BR, Findell KL (2012) Scaling in surface hydrology:
761 Progress and challenges. J Contemp Water Res Educ 147(1):28-40
762 https://doi.org/10.1111/j.1936-704X.2012.03105.x
763 Grangeon T, Vandromme R, Cerdan O, De Girolamo AM, Lo Porto A (2021)
764 Modelling forest fire and firebreak scenarios in a Mediterranean mountainous
765 catchment: Impacts on sediment loads. J Environ Manag 289:112497
766 https://doi.org/10.1016/j.jenvman.2021.112497
767 Grangeon T, Vandromme R, Pak LT, Martin P, Cerdan O, Richet JB, Evrard O,
768 Souchère V, Auzet AV, Ludwig B, Ouvry JF. Dynamic parameterization of soil surface
769 characteristics for hydrological models in agricultural catchments. Submitted to Catena
770 Gruber S, Peckham S (2009) Land-surface parameters and objects in hydrology. In:
771 Hengl T, Reuter HI (eds) Geomorphometry: Concepts, Software, Applications. Elsevier,
772 Amsterdam, pp 171-194
773 Haddadchi A, Ryder DS, Evrard O, Olley J (2013) Sediment fingerprinting in fluvial
774 systems: review of tracers, sediment sources and mixing models. Int J Sediment
775 Res 28(4):560-578 https://doi.org/10.1016/S1001-6279(14)60013-5

IUSS Working Group WRB (2015) World reference base for soil resources 2014, update 2015: International soil classification system for naming soils and creating legends for soil maps. World Soil Resour Rep 106:192

Ivanciuc O (2007) Applications of support vector machines in chemistry. Rev Comput Chem 23:291 https://doi.org/10.1002/9780470116449.ch6

Jancewicz K, Migoń P, Kasprzak M (2019) Connectivity patterns in contrasting types of tableland sandstone relief revealed by Topographic Wetness Index. Sci Total Environ 656:1046-1062 https://doi.org/10.1016/j.scitotenv.2018.11.467

Julien PY (1995) Erosion and sedimentation. Cambridge University Press

Karydas C, Panagos P, Gitas IZ (2014) A classification of water erosion models according to their geospatial characteristics. Int J Digit Earth 7(3):229-250 https://doi.org/10.1080/17538947.2012.671380

Laceby JP, Evrard O, Smith HG, Blake WH, Olley JM, Minella JP, Owens PN (2017) The challenges and opportunities of addressing particle size effects in sediment source fingerprinting: a review. Earth-Sci Rev 169:85-103 https://doi.org/10.1016/j.earscirev.2017.04.009

Landemaine V (2016) Érosion des sols et transferts sédimentaires sur les bassins versants de l'Ouest du Bassin de Paris: analyse, quantification et modélisation à l'échelle pluriannuelle. Thesis, Normandie Universitè

Lemma H, Frankl A, Griensven A, Poesen J, Adgo E, Nyssen J (2019) Identifying erosion hotspots in Lake Tana Basin from a multisite Soil and Water Assessment Tool validation: Opportunity for land managers. Land Degrad Dev 30:1449–1467 https://doi.org/10.1002/ldr.3332

Londero AL, Minella JPG, Deuschle D, Schneider FJA, Boeni M, Merten GH (2017) Impact of broad-based terraces on water and sediment losses in no-till (paired zero-order) catchments in southern Brazil. J Soils Sediments 18(3):1159-1175 https://doi.org/10.1007/s11368-017-1894-y

Londero AL, Minella JPG, Schneider FJA, Deuschle D, Menezes D, Evrard O, Boeni M, Merten GH (2021a) Quantifying the impact of no-till on runoff in southern Brazil at hillslope and catchment scales. Hydrol Process 35(3):e14094 https://doi.org/10.1002/hyp.14094

Londero AL, Minella JPG, Schneider FJA, Deuschle D, Merten GH, Evrard O, Boeni M (2021b) Quantifying the impact of no-till on sediment yield in southern Brazil at

809 hillslope and catchment scales. Hydrol Process 35(7):e14286
810 https://doi.org/10.1002/hyp.14286
811 Martínez-Carreras N, Krein A, Udelhoven T, Gallart F, Iffly JF, Hoffmann L, Pfister L,
812 Walling DE (2010) A rapid spectral-reflectance-based fingerprinting approach for
813 documenting suspended sediment sources during storm runoff events. J Soils Sediments
814 10:400-413 https://doi.org/10.1007/s11368-009-0162-1
815 Merritt WS, Letcher RA, Jakeman AJ (2003) A review of erosion and sediment
816 transport models. Environ Model Softw 18(8-9):761-799 https://doi.org/10.1016/S1364-
817 8152(03)00078-1
818 Meyer D, Dimitriadou E, Hornik K, Weingessel A, Leisch F, Chang CC, Lin CC (2014)
819 e1071: Misc functions of the Department of Statistics (e1071), TU Wien. R package
820 version 1(3)
821 Mhiret DA, Dagnew DC, Assefa TT, Tilahun SA, Zaitchik BF, Steenhuis TS (2019)
822 Erosion hotspot identification in the sub-humid Ethiopian highlands. Ecohydrol
823 Hydrobiol 19(1):146-154 https://doi.org/10.1016/j.ecohyd.2018.08.004
824 Minella JP, Walling DE, Merten GH (2014) Establishing a sediment budget for a small
825 agricultural catchment in southern Brazil, to support the development of effective
826 sediment management strategies. J Hydrol 519:2189-2201
827 https://doi.org/10.1016/j.jhydrol.2014.10.013
828 Mitasova H, Hofierka J, Zlocha M, Iverson LR (1996) Modelling topographic potential
829 for erosion and deposition using GIS. Int J Geogr Inf Syst 10(5):629-641
830 https://doi.org/10.1080/02693799608902101
831 Momm HG, Bingner RL, Wells RR, Wilcox D (2012) AGNPS GIS-based tool for
832 watershed-scale identification and mapping of cropland potential ephemeral
833 gullies. Appl Eng Agri 28(1):17-29 https://doi.org/10.13031/2013.41282
834 Moore ID, Grayson RB, Ladson AR (1991) Digital Terrain Modelling: a review of
835 hydrological, geomorphological, and biological applications. Hydrol Process 5:3-30
836 https://doi.org/10.1002/hyp.3360050103
837 Nearing MA, Jetten V, Baffaut C, Cerdan O, Couturier A, Hernandez M, Le Bissonnais
838 Y, Nichols MH, Nunes JP, Renschler CS, Sourchère V (2005) Modeling response of
839 soil erosion and runoff to changes in precipitation and cover. Catena 61(2-3):131-154
840 Owens PN, Blake WH, Gaspar L, Gateuille D, Koiter AJ, Lobb DA, Petticrew EL,
841 Reiffarth D, Smith HG, Woodward JC (2016) Fingerprinting and tracing the sources of
842 soils and sediments: earth and ocean science, geoarchaeological, forensic, and human

health applications. Earth-Sci Rev 162:1-23
https://doi.org/10.1016/j.earscirev.2016.08.012
Palazón L, Latorre B, Gaspar L, Blake WH, Smith HG, Navas A (2016) Combining catchment modelling and sediment fingerprinting to assess sediment dynamics in a Spanish Pyrenean river system. Sci Total Environ 569:1136-1148
https://doi.org/10.1016/j.scitotenv.2016.06.189
Patault E, Landemaine V, Ledun J, Soulignac A, Fournier M, Ouvry JF, Cerdan O, Laignel B (2020) Predicting Sediment Discharge at Water Treatment Plant Under Different Land Use Scenarios Coupling Expert-Based GIS Model and Deep Neural Network. Hydrol Earth Syst Sci Discuss 1-26 https://doi.org/10.5194/hess-2020-363
Pedron FA, Dalmolin RSD, Moura-Bueno JM, Schenato RB, Soligo MF, Nalin RS, Freitas HM (2021) Levantamento detalhado de solo da bacia do arroio Guarda Mor. MSRS, Santa Maria
Poulenard J, Perrette Y, Fanget B, Quetin P, Trevisan D, Dorioz JM (2009) Infrared spectroscopy tracing of sediment sources in a small rural watershed (French Alps). Sci Total Environ 407:2808-2819 https://doi.org/10.1016/j.scitotenv.2008.12.049
QGIS Development Team (2020) QGIS Geographic Information System. Open Source Geospatial Foundation Project https://qgis.org
Qiu Z, Hall C, Drewes D, Messinger G, Prato T, Hale K, Van Abs D (2014) Hydrologically sensitive areas, land use controls, and protection of healthy watersheds. J Water Resour Plan Manag 140(7):04014011
https://doi.org/10.1061/(ASCE)WR.1943-5452.0000376
Rossetti L, Lima EF, Waichel BL, Hole MJ, Simões MS, Scherer CM (2018) Lithostratigraphy and volcanology of the Serra Geral Group, Paraná-Etendeka Igneous Province in southern Brazil: Towards a formal stratigraphical framework. J Volcanol Geotherm Res 355:98-114 https://doi.org/10.1016/j.jvolgeores.2017.05.008
Sari V, Paiva EMCDD, Paiva JBDD (2016) Interceptação da chuva em diferentes formações florestais na região sul do Brasil. Rev Bras Recur Hidr 21(1):65-79
https://doi.org/10.21168/rbrh.v21n1.p65-79
Savitzky A, Golay MJE (1964) Smoothing and differentiation of data by simplified least squares procedures. Anal Chem 36:1627-1639 https://doi.org/10.1021/ac60214a047
Schneider FJA (2021) Modeling sediment yield on hillslopes under no-till farming. Thesis, Universidade Federal de Santa Maria

876 Silva CC, Minella JPG, Schlesner A, Merten GH, Barros CAP, Tassi R, Dambroz APB
877 (2021) Unpaved road conservation planning at the catchment scale. Environ Monit
878 Assess 193(9):1-23 https://doi.org/10.1007/s10661-021-09398-z
879 Stevens A, Ramirez-Lopez L (2013) An introduction to the prospectr package. R
880 package Vignette R package version 0.1.3
881 Teng HF, Hu J, Zhou Y, Zhou LQ, Shi Z (2019) Modelling and mapping soil erosion
882 potential in China. J Integr Agric 18(2):251-264 https://doi.org/10.1016/S2095-
883 3119(18)62045-3
884 Thomaz EL, Peretto GT (2016) Hydrogeomorphic connectivity on roads crossing in
885 rural headwaters and its effect on stream dynamics. Sci Total Environ 550:547-555
886 https://doi.org/10.1016/j.scitotenv.2016.01.100
887 Thomaz EL, Vestena LR, Ramos Scharrón CE (2014) The effects of unpaved roads on
888 suspended sediment concentration at varying spatial scales–a case study from Southern
889 Brazil. Water Environ J 28(4):547-555 https://doi.org/10.1111/wej.12070
890 Tiecher T, Caner L, Minella JPG, Bender MA, Santos DR (2016) Tracing sediment
891 sources in a subtropical rural catchment of southern Brazil by using geochemical tracers
892 and near-infrared spectroscopy. Soil Tillage Res 156:478-491
893 https://doi.org/10.1016/j.still.2015.03.001
894 Tiecher T, Minella JPG, Evrard O, Caner L, Merten GH, Capoane V, Didoné EJ, Santos
895 DR (2018) Fingerprinting sediment sources in a large agricultural catchment under no-
896 tillage in Southern Brazil (Conceição River). Land Degrad Dev 29(4):939-951
897 https://doi.org/10.1002/ldr.2917
898 Tiecher T, Moura-Bueno JM, Caner L, Minella JP, Evrard O, Ramon R, Naibo G,
899 Barros CA, Silva YJ, Amorim FF, Rheinheimer DS (2021) Improving the quantification
900 of sediment source contributions using different mathematical models and spectral
901 preprocessing techniques for individual or combined spectra of ultraviolet–visible, near-
902 and middle-infrared spectroscopy. Geoderma 384:114815
903 https://doi.org/10.1016/j.geoderma.2020.114815
904 Uber M, Nord G, Legout C, Cea L (2021) How do modeling choices and erosion zone
905 locations impact the representation of connectivity and the dynamics of suspended
906 sediments in a multi-source soil erosion model?. Earth Surface Dynamics 9(1):123-44
907 https://doi.org/10.5194/esurf-9-123-2021
908 Vaissie P, Monge A, Husson F (2020) Perform Factorial Analysis from 'FactoMineR'
909 with a Shiny Application. Package 'Factoshiny' version 2.2

910 Verheyen D, Diels J, Kissi E, Poesen J (2014) The use of visible and near-infrared
911 reflectance measurements for identifying the source of suspended sediment in rivers and
912 comparison with geochemical fingerprinting. J Soils Sediments 14(11):1869-1885
913 https://doi.org/10.1007/s11368-014-0938-9
914 Vijith H, Dodge-Wan D (2019) Modelling terrain erosion susceptibility of logged and
915 regenerated forested region in northern Borneo through the Analytical Hierarchy
916 Process (AHP) and GIS techniques. Geoenvironmental Disasters 6(1):8
917 https://doi.org/10.1186/s40677-019-0124-x
918 Viscarra Rossel RA, Behrens T (2010) Using data mining to model and interpret soil
919 diffuse reflectance spectra. Geoderma 158(1-2):46-54
920 https://doi.org/10.1016/j.geoderma.2009.12.025
921 Viscarra Rossel RA, Walvoort DJJ, McBratney AB, Janik LJ, Skjemstad JO (2006)
922 Visible, near infrared, mid infrared or combined diffuse reflectance spectroscopy for
923 simultaneous assessment of various soil properties. Geoderma 131(1-2):59-75
924 https://doi.org/1016/j.geoderma.2005.03.007
925 Walling DE (2013) The evolution of sediment source fingerprinting investigations in
926 fluvial systems. J Soils Sediments 13:1658-1675 https://doi.org/10.1007/s11368-013-
927 0767-2
928 Walling DE (1983) The sediment delivery problem. J Hydrol 65(1-3):209-237
929 https://doi.org/10.1016/0022-1694(83)90217-2
930 Wildner W, Ramgrab GE, Lopes RC, Iglesias CMF (2008) Mapa Geológico do Estado
931 do Rio Grande do Sul (1:750,000) Porto Alegre: Serviço Geológico do Brasil
932 Wilson JP, Gallant JC (2000) Digital terrain analysis. Terrain analysis: Principles and
933 applications 6(12):1-27
934 Wohl E, Brierley G, Cadol D et al (2019) Connectivity as an emergent property of
935 geomorphic systems. Earth Surf Process Landf 44(1):4-26
936 https://doi.org/10.1002/esp.4434
937 Zevenbergen LW, Thorne CR (1987) Quantitative analysis of land surface
938 topography. Earth Surf Process Landf 12(1):47-56
939 https://doi.org/10.1002/esp.3290120107
940 Ziegler AD, Sutherland RA, Giambelluca TW (2000) Runoff generation and sediment
941 production on unpaved roads, footpaths and agricultural land surfaces in northern
942 Thailand. Earth Surf Process Landf 25(5):519-534 https://doi.org/10.1002/(SICI)1096-
943 9837(200005)25:5<519::AID-ESP80>3.0.CO;2-T

Tables

Table 1. Rainfall events characteristics.

	Rainfall event	Rainfall (mm)	Duration time (minutes)	Previous rainfall (48 hours)
1	08 October 2015	35	84	43.68
2	19 November 2015	80	222	14.07
3	14 December 2015	36	522	46.62
4	29 December 2015	25	168	16.8

Table 2. Number of potential sediment source samples and sediment samples.

Catchment/ Sources	Source samples						Sediment samples
	Crop fields	Unpaved Road	Stream Channel	Grassland	Forest	Total	Riverbed sediment
S1	8	9	9	7	6	39	7
S2	14	9	6	6	6	41	6
S3	6	6	6	6	6	30	6
GMex	-	-	-	-	-	-	6
Total	28	24	21	19	18	110	15

Table 3. Support Vector Machine models calibration and validation performance for measured and predicted artificial mixtures composition.

	Sources	Performance indicator	Calibration	Validation
GMex	S1	R^2	1	0.58
		RMSE	2.75	25.46
		ME	0.34	-8.28
	S2	R^2	1	0.93
		RMSE	3.11	12.63
		ME	0.59	7.65
	S3	R^2	1	0.37
		RMSE	2.95	26.59
		ME	0.52	2.38
S1	Topsoil	R^2	1	0.36
		RMSE	3.31	20.01
		ME	0.19	3.43
	Stream channel	R^2	1	0.37
		RMSE	2.66	20.5

		ME	1.32	0.52
	Unpaved roads	R^2	1	0.92
		RMSE	2.58	6.52
		ME	0.84	2.76
	Forest	R^2	0.99	0.9
		RMSE	2.38	15.65
		ME	0.57	-3.5
S2	Topsoil	R^2	1	0.32
		RMSE	3.42	21.54
		ME	0.45	3.23
	Stream channel	R^2	1	0.37
		RMSE	2.6	19.63
		ME	0.95	1.4
	Unpaved roads	R^2	0.99	0.8
		RMSE	2.66	9.03
		ME	0.58	4.4
	Forest	R^2	0.99	0.29
		RMSE	2.57	24.76
		ME	0.7	-5.92
S3	Topsoil	R^2	1	0.28
		RMSE	3.38	22.06
		ME	0.22	7.68
	Stream channel	R^2	1	0.39
		RMSE	2.63	18.76
		ME	0.96	-0.1
	Unpaved roads	R^2	1	0.93
		RMSE	2.53	5.04
		ME	0.05	0.92
	Forest	R^2	0.99	0.71
		RMSE	2.74	23.23
		ME	0.91	-6

Figure Captions

Fig. 1 Location of Guarda Mor catchment, Júlio de Castilhos' rainfall-runoff monitoring station and ANA's weather station number 2953008 within the state of Rio Grande do Sul. In detail, soil and sediment sampling sites at Guarda Mor catchment

Fig. 2 Guarda Mor catchment. **a** Digital elevation map. **b** Pedological and **c** geological maps. **d** Land use classification map

Fig. 3 Maps of Topographic Wetness Index (TWI), Stream Power Index (SPI) and LS Factor

Fig. 4 Frequency histograms for Topographic Wetness Index (TWI), LS Factor, Stream Power Index (SPI) and Slope of sub catchments and GMex

968 **Fig. 5** Boxplots of zonal statistics analysis for topographic attributes (LS Factor, Slope,
969 Stream Power Index – SPI, Topographic Wetness Index – TWI and Plan Curvature) and
970 land uses in sub catchments 1, 2 and 3
971 **Fig. 6** Comparison between higher TWI (**a** and **b**) and SPI (**c** and **d**) values and satellite
972 images in crop fields of sub catchment 1.
973 **Fig. 7** WaterSed output maps for runoff and erosion in the three sub catchments, for
974 events 1, 2, 3 and 4
975 **Fig. 8** Zonal statistics for diffuse erosion estimates and land uses in sub catchments 1, 2
976 and 3
977 **Fig. 9** Boxplots for sediment source contribution in Fingerprinting 1 (**a**) and
978 Fingerprinting 2 (**b** = S1, **c** = S2, **d** = S3)
979 **Fig. 10** Individuals factor map from Principal Components Analysis for sediment
980 samples for the outlets of sub catchments 1, 2 and 3, and GMex

Fig. 1

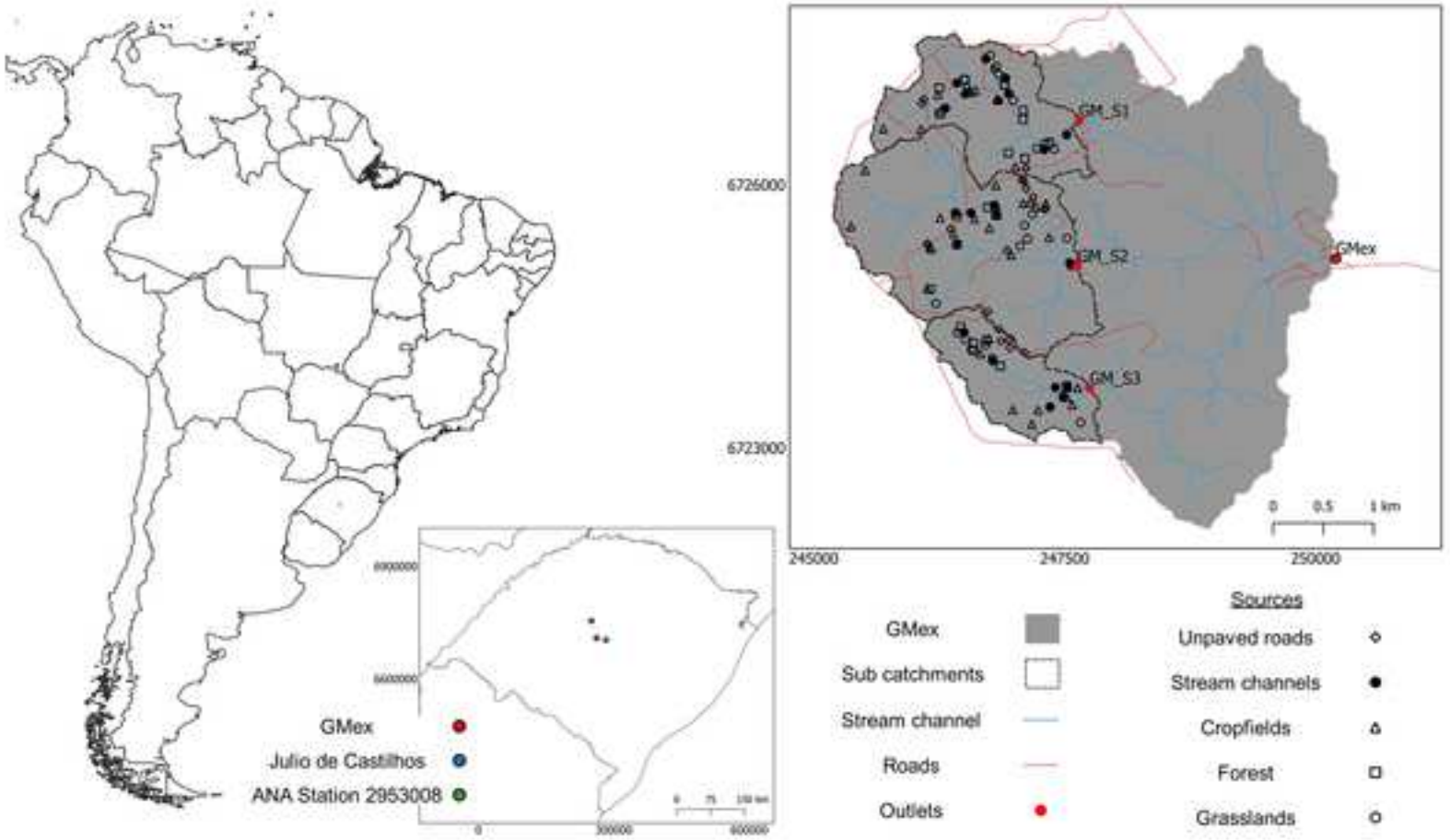

Fig. 2

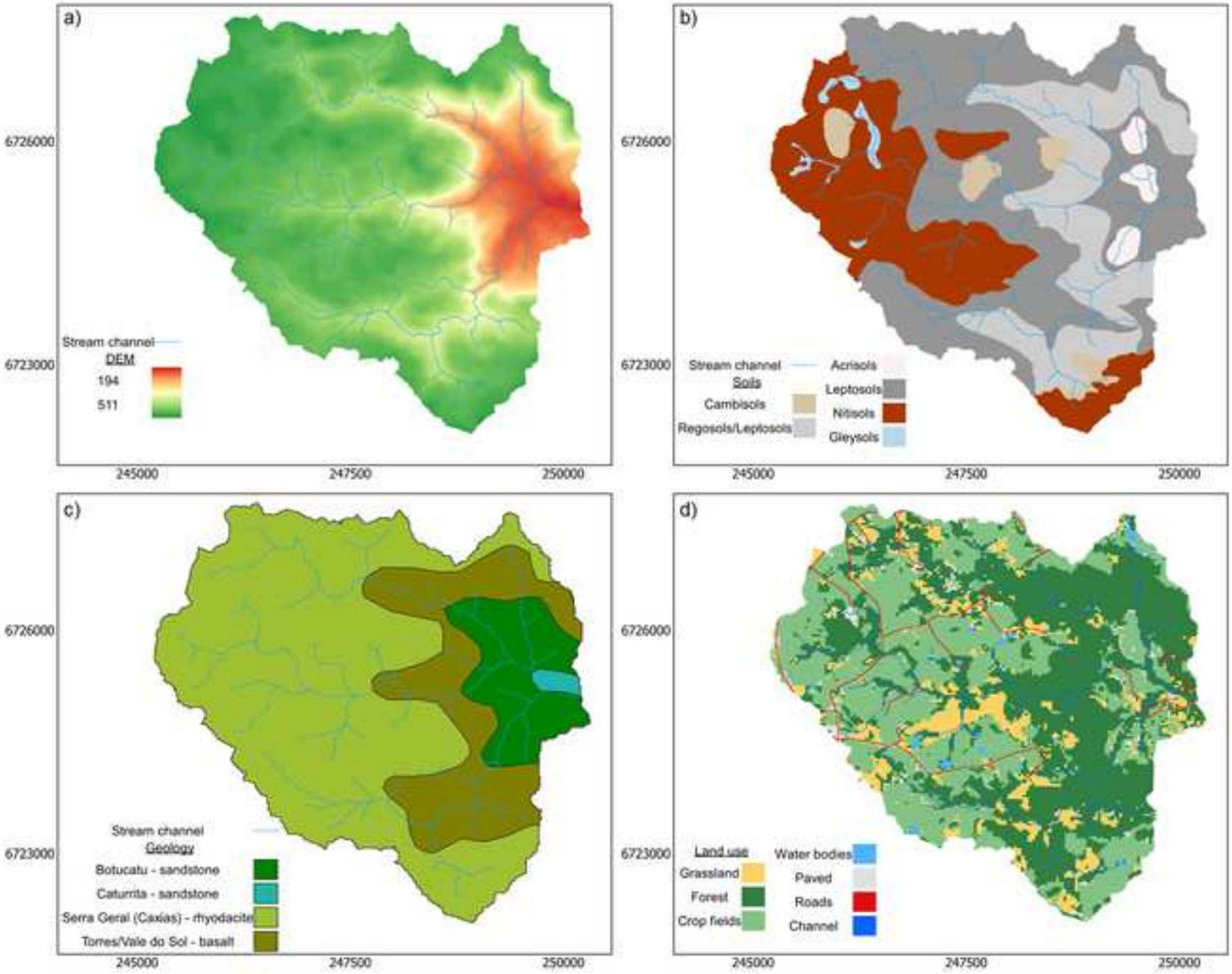

Fig. 3

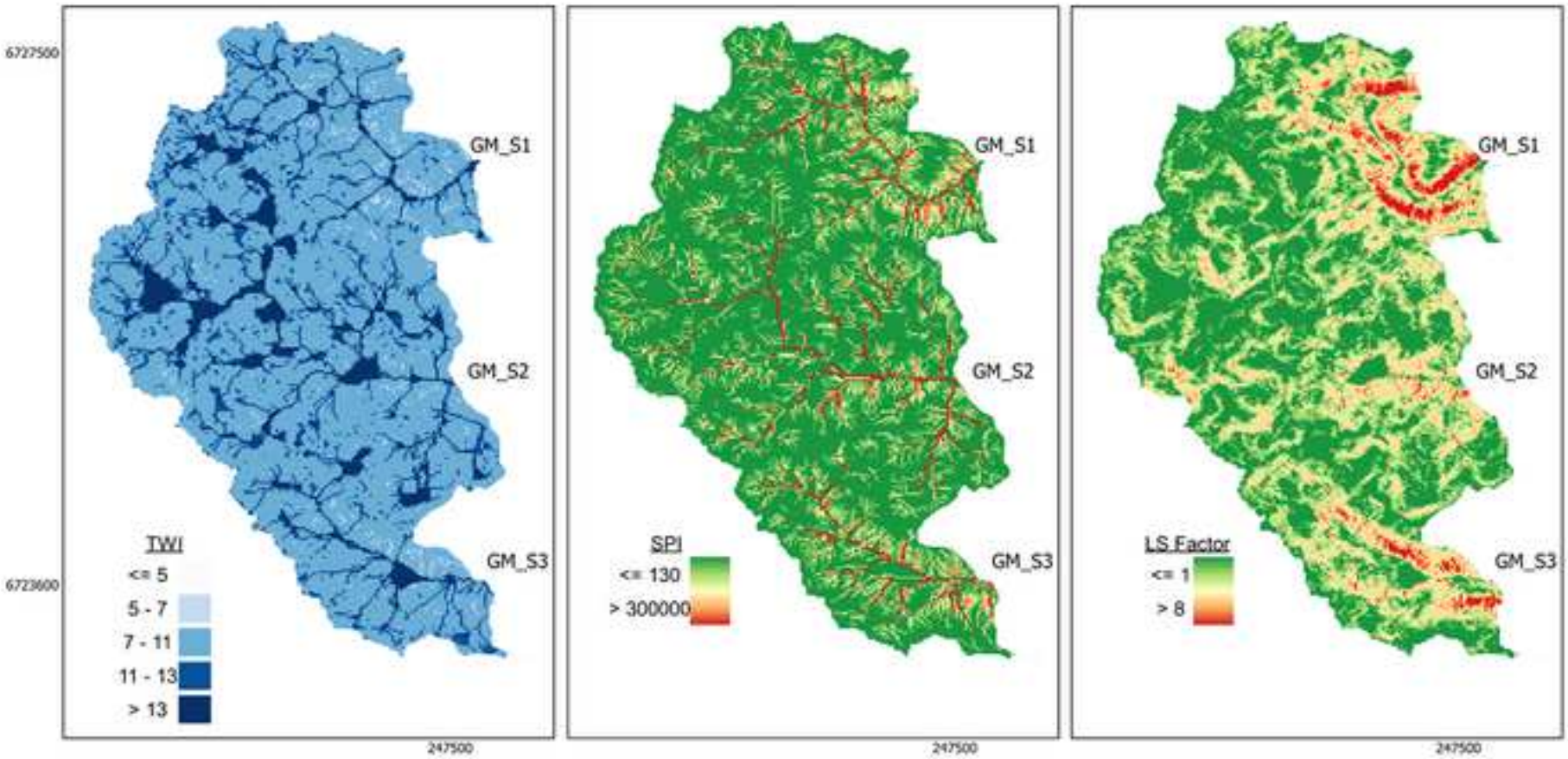

Fig. 4

Click here to access/download;Figure;Fig4.tiff

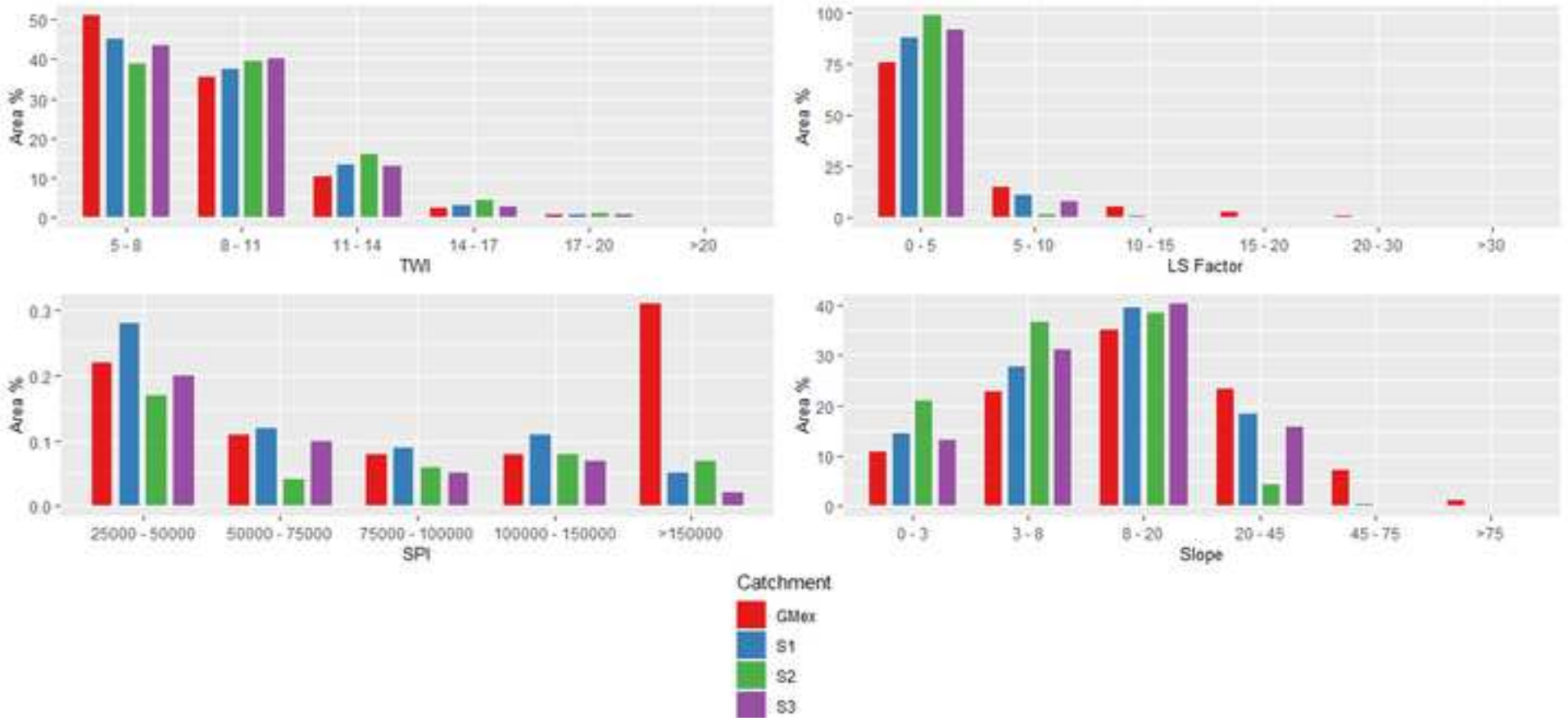

Fig. 5

Click here to access/download;Figure;Fig5.tiff

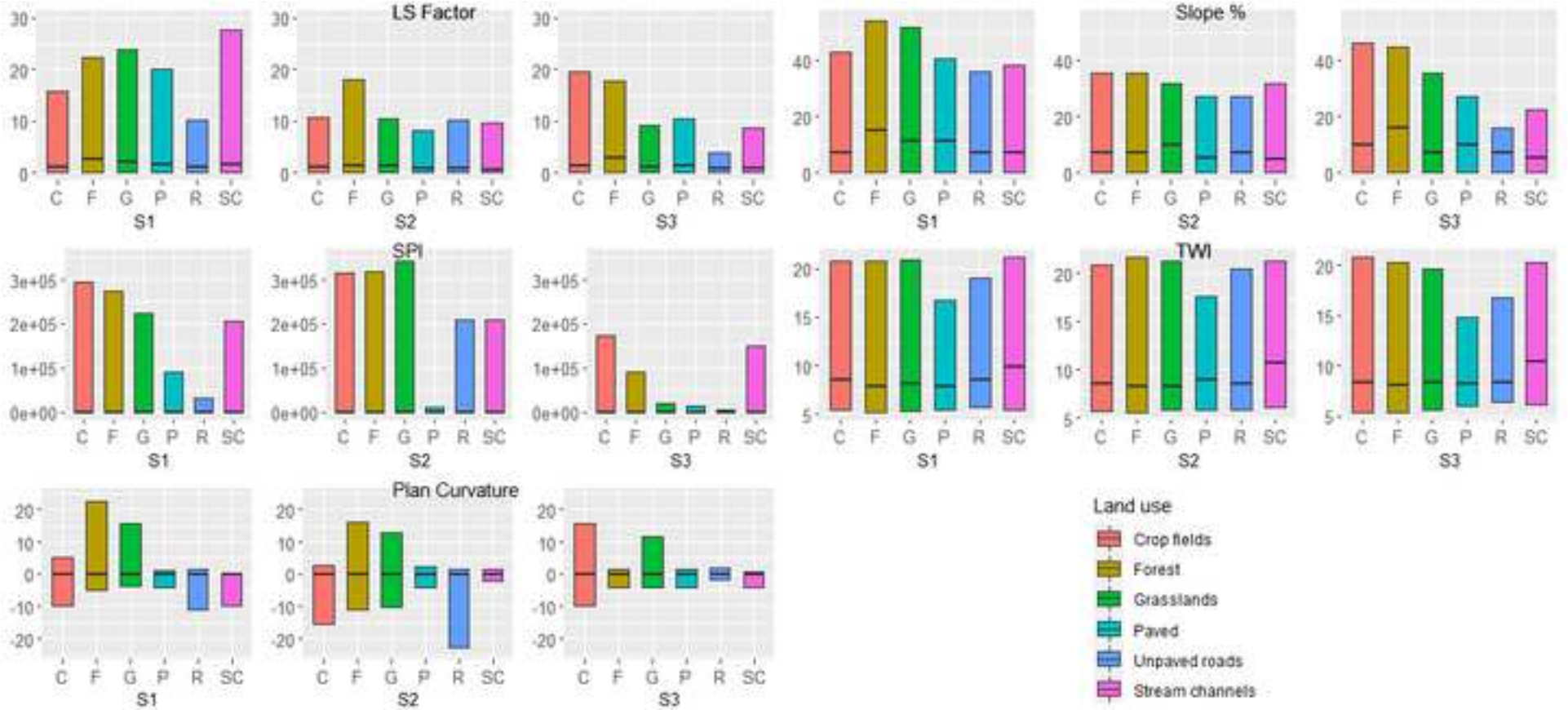

Fig. 6

Click here to access/download;Figure;Fig6.tif

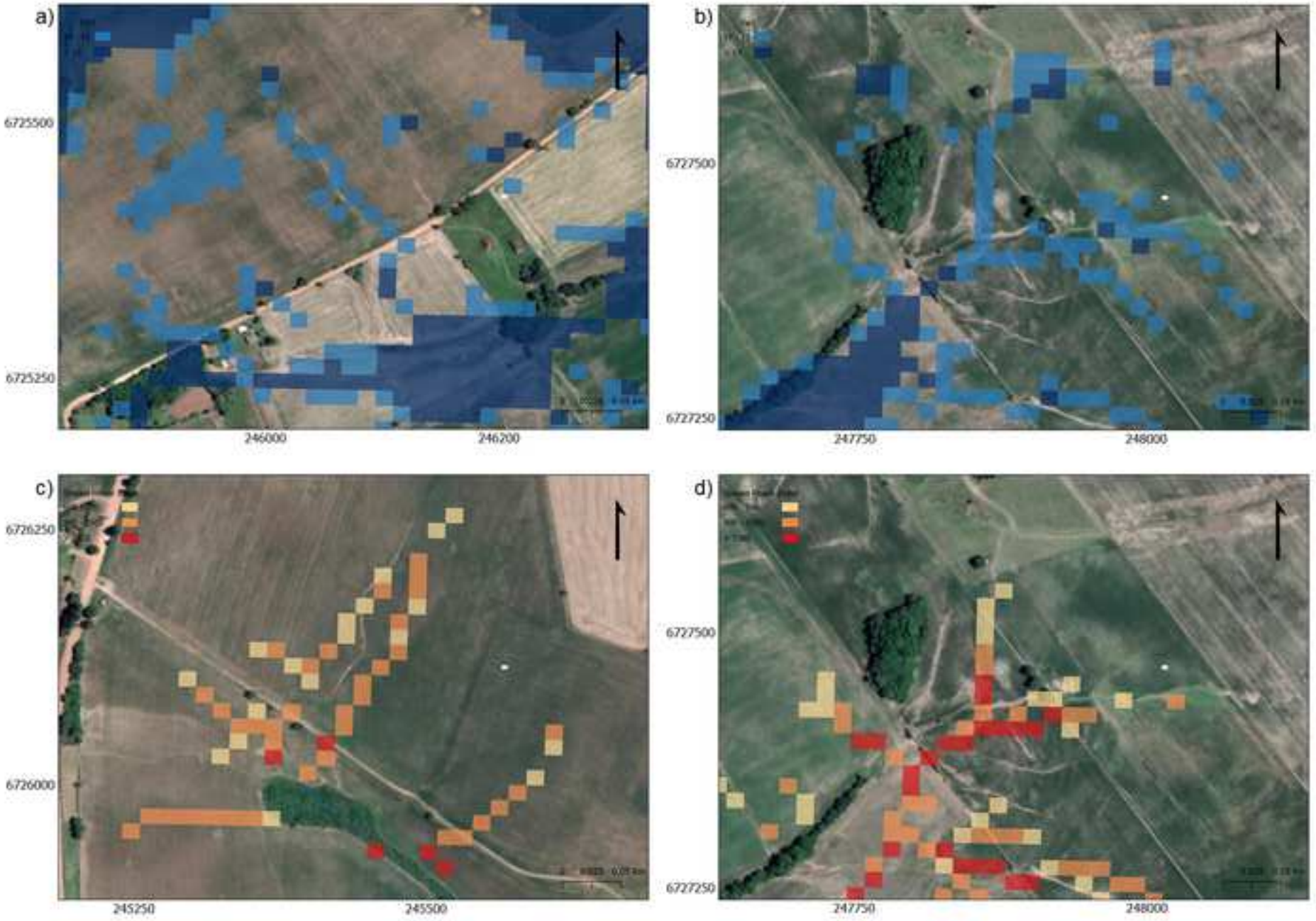

Fig. 7

Click here to access/download;Figure;Fig7.tif

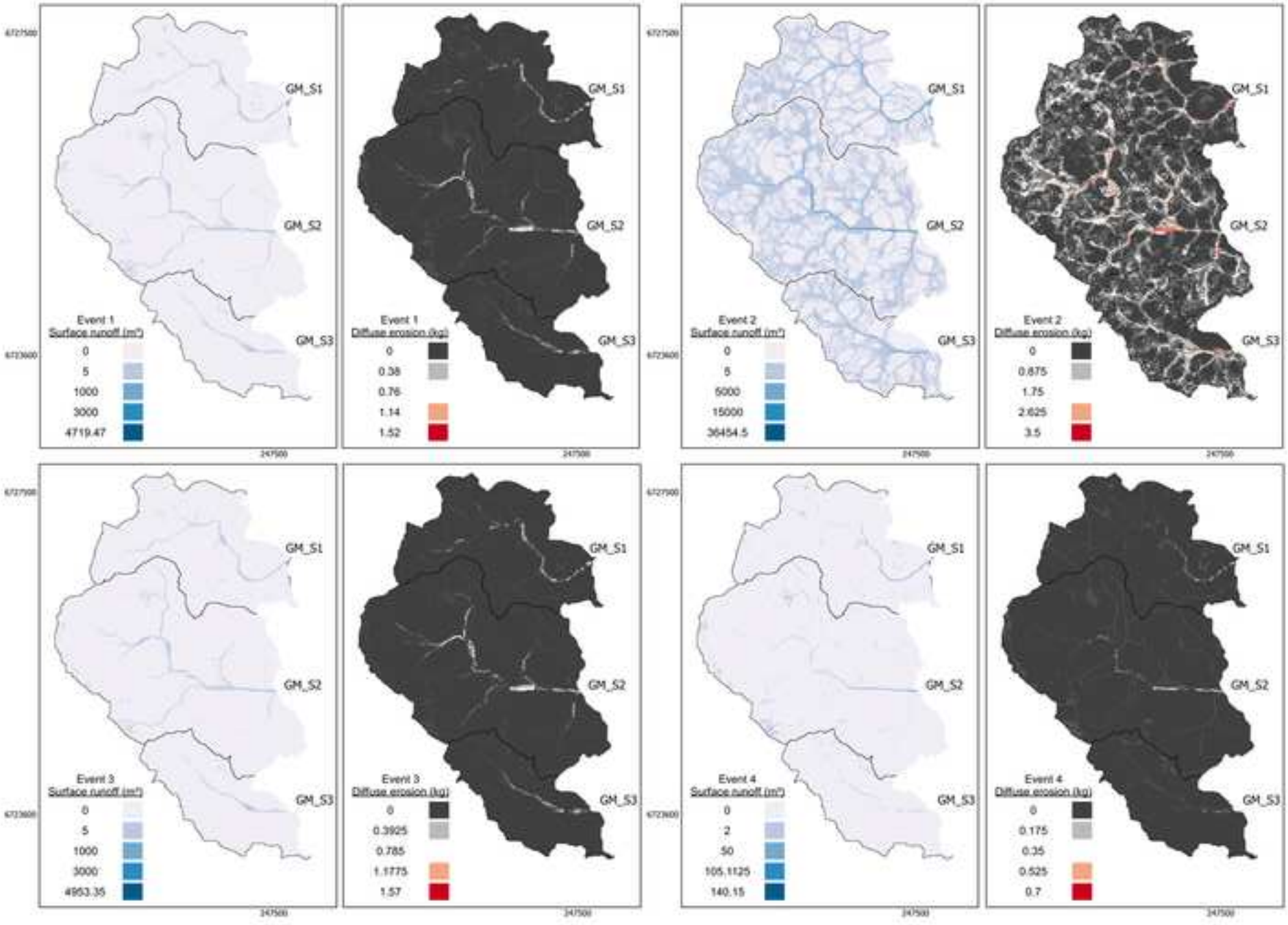

Fig. 8

Click here to access/download;Figure;Fig8.tiff

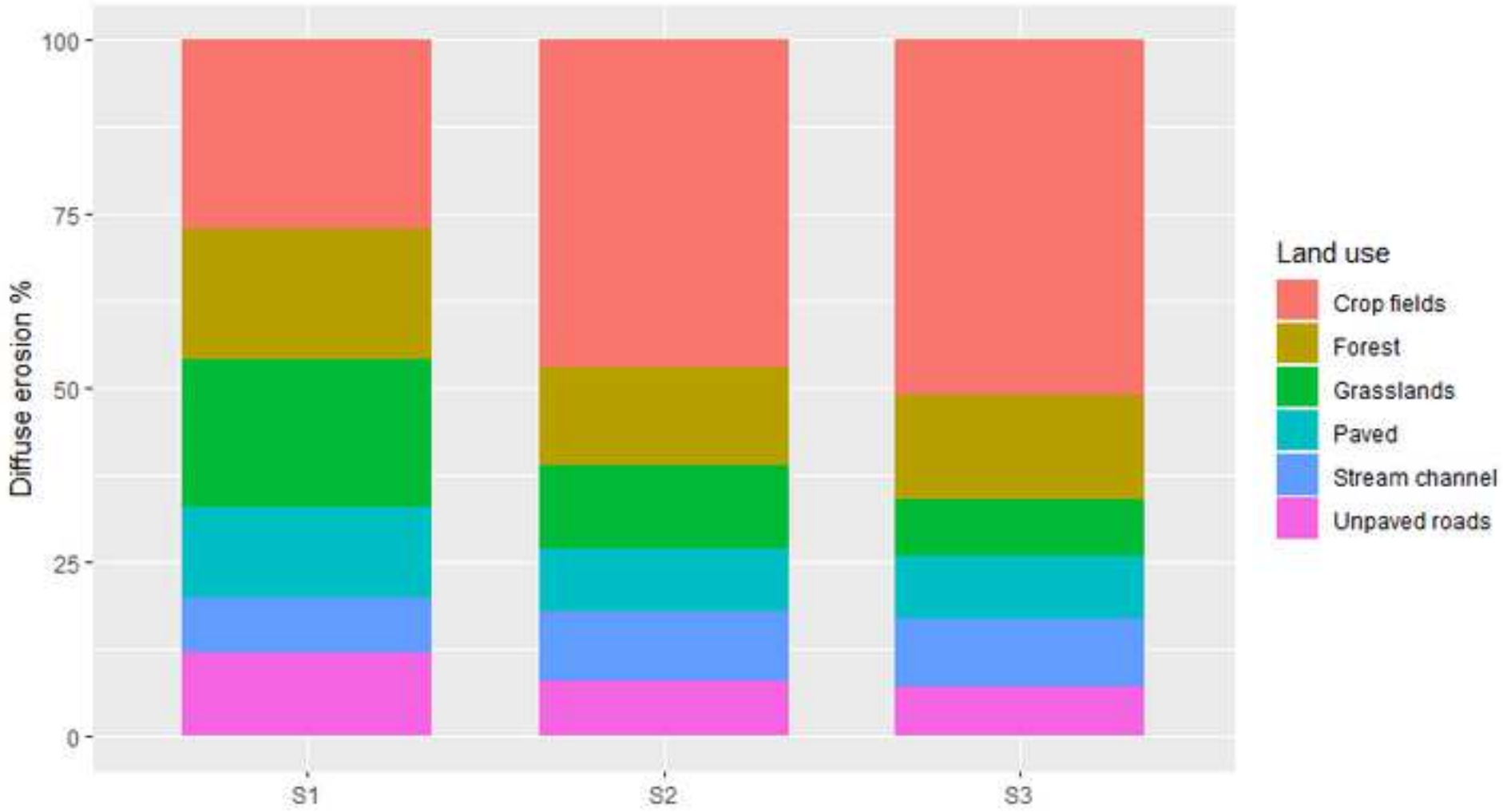

Fig. 9

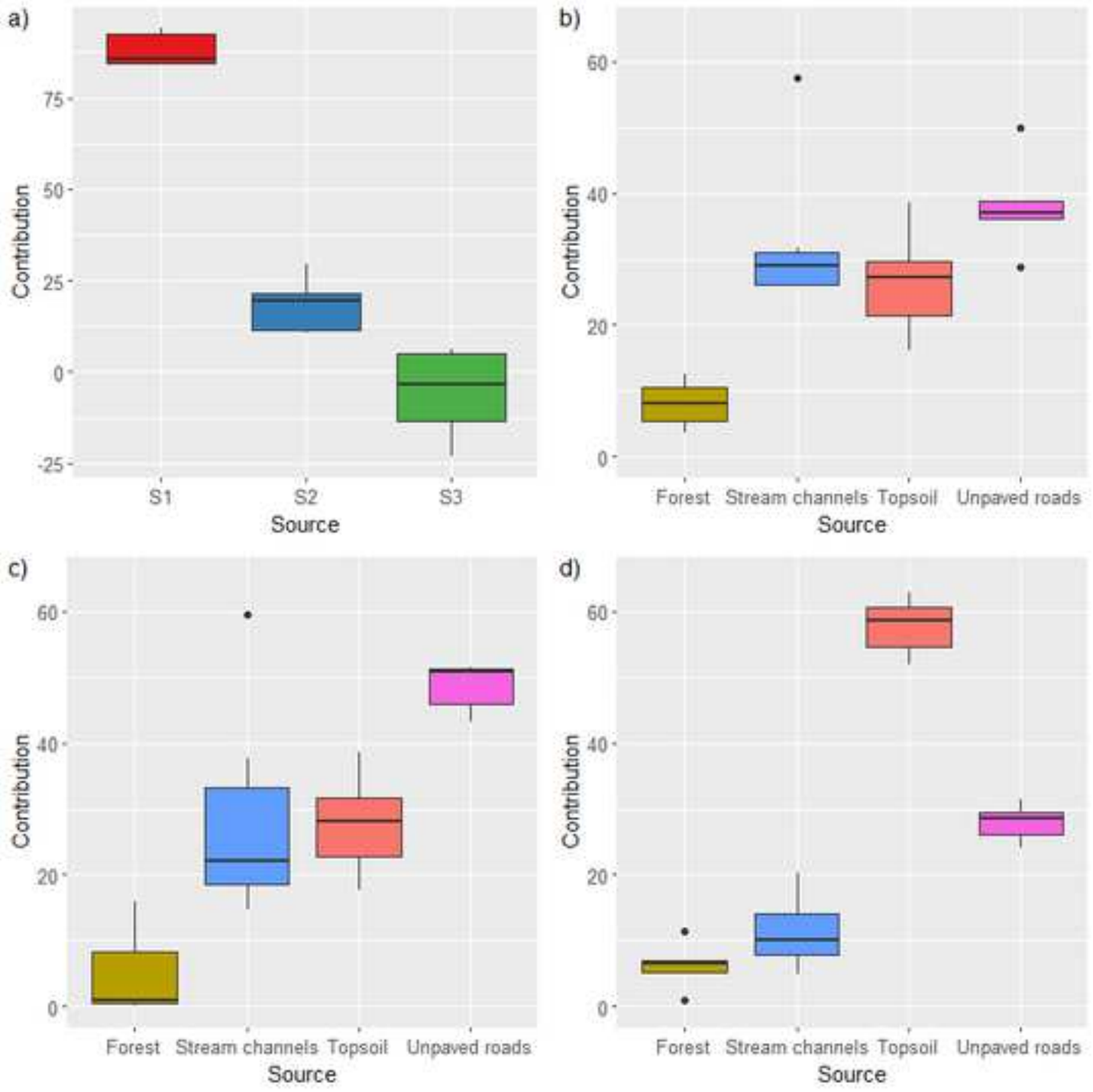

Fig. 10

Click here to access/download;Figure;Fig10.tif